International Journal of *Geo-Information*

MDPI

Article

How Has the Recent Climate Change Affected the Spatiotemporal Variation of Reference Evapotranspiration in a Climate Transitional Zone of Eastern China?

Meng Li [1,2,†], Ronghao Chu [3,4,5,*,†], Xiuzhu Sha [6], Abu Reza Md. Towfiqul Islam [7], Yuelin Jiang [2] and Shuanghe Shen [8]

1 School of Civil Aviation, Zhengzhou University of Aeronautics, Zhengzhou 450046, China
2 School of Resources and Environment, Anhui Agricultural University, Hefei 230036, China
3 China Meteorological Administration·Henan Key Laboratory of Agrometeorological Support and Applied Technique, Zhengzhou 450003, China
4 Henan Institute of Meteorological Sciences, Zhengzhou 450003, China
5 Anhui Public Meteorological Service Center, Anhui Meteorological Bureau, Hefei 230031, China
6 The Weather Modification Center of Henan Province, Zhengzhou 450003, China
7 Department of Disaster Management, Begum Rokeya University, Rangpur 5400, Bangladesh
8 Key Laboratory of Meteorological Disaster, Ministry of Education (KLME), Joint International Research Laboratory of Climate and Environment Change (ILCEC), Collaborative Innovation Center on Forecast and Evaluation of Meteorological Disasters (CIC-FEMD), Jiangsu Key Laboratory of Agricultural Meteorology, College of Applied Meteorology, Nanjing University of Information Science & Technology, Nanjing 210044, China
* Correspondence: ronghao_chu@163.com
† These authors contributed equally to this work.

check for updates

Citation: Li, M.; Chu, R.; Sha, X.; Islam, A.R.M.T.; Jiang, Y.; Shen, S. How Has the Recent Climate Change Affected the Spatiotemporal Variation of Reference Evapotranspiration in a Climate Transitional Zone of Eastern China? *ISPRS Int. J. Geo-Inf.* **2022**, *11*, 300. https://doi.org/10.3390/ijgi11050300

Academic Editors: Wolfgang Kainz and Godwin Yeboah

Received: 20 March 2022
Accepted: 2 May 2022
Published: 6 May 2022
Corrected: 8 March 2023

Abstract: Reference evapotranspiration (ET_0) is essential for agricultural production and crop water management. The recent climate change affecting the spatiotemporal variation of ET_0 in eastern China continues to still be less understood. For this purpose, the latest observed data from 77 meteorological stations in Anhui province were utilized to determine the spatiotemporal variations of ET_0 by the use of the Penman–Monteith FAO 56 (PMF-56) model. Furthermore, the Theil–Sen estimator and the Mann–Kendall (M–K) test were adopted to analyze the trends of ET_0 and meteorological factors. Moreover, the differential method was employed to explore the sensitivity of ET_0 to meteorological factors and the contributions of meteorological factors to ET_0 trends. Results show that the ET_0 decreased significantly before 1990, and then increased slowly. The ET_0 is commonly higher in the north and lower in the south. ET_0 is most sensitive to relative humidity (RH), except in summer. However, in summer, net radiation (R_n) is the most sensitive factor. During 1961–1990, R_n was the leading factor annually, during the growing season and summer, while wind speed (u_2) played a leading role in others. All meteorological factors provide negative contributions to ET_0 trends, which ultimately lead to decreasing ET_0 trends. During 1991–2019, the leading factor of ET_0 trends changed to the mean temperature (T_a) annually, during the growing season, spring and summer, and then to R_n in others. Overall, the negative contributions from u_2 and R_n cannot offset the positive contributions from T_a and RH, which ultimately lead to slow upward ET_0 trends. The dramatic drop in the amount of u_2 that contributes to the changes in ET_0 in Region III is also worth noting.

Keywords: climate change; reference evapotranspiration; sensitivity coefficient; differential method; water resources management; eastern China

1. Introduction

Evapotranspiration (ET) is a crucial portion of the hydrologic cycle. It participates in surface runoff, groundwater recharge and other key processes, and plays a pivotal role in climate change, hydrological research and irrigation water management [1–3]. Reference crop evapotranspiration (ET_0) is the potential evapotranspiration that is further specified in terms of crop characteristics. Doorenbos et al. [4] defined ET_0 as the ET of vast grassland with uniform and normal growth, completely covering the surface and providing sufficient water at a height of 8–15 cm. Subsequently, Allen et al. [5] introduced the concept of ET_0 and defined it as the ET of an ideal 12 cm crop with a fixed canopy resistance of 70 $s \cdot m^{-1}$ and an albedo of 0.23 (very similar to green grassland with an open surface, uniform height, vigorous growth, complete coverage of the ground and a sufficient supply of soil moisture). Since then, ET_0 has been widely used in the fields of agronomy, agriculture, irrigation and ecology [6].

Currently, the Penman–Monteith FAO (the Food and Agriculture Organization of the United Nations) 56 (PMF-56) model, a modified Monteith equation [7], has been used broadly for estimating ET_0 worldwide based on its solid theoretical base and wide applications [8]. In the PMF-56 model, the climatic factors (i.e., temperature, humidity, wind speed and radiation) are the main influencing elements for ET_0. However, in recent decades, climate change, especially global warming, has stimulated worldwide concerns [9–11], which have also led to changes in ET_0 in different parts of the world [12–16]. Although under the influence of global warming, ET_0 is not only affected by temperature, but also by other elements, and the coupling of multiple factors ultimately determines the increasing or decreasing trends of ET_0. Therefore, quantifying the impact of meteorological factors on ET_0 trends is very essential. In recent studies, quantitative methods have mainly been used to assess the effects of meteorological factors on ET_0 trends, for example, the multiple regression analysis [17], partial correlation analysis and stepwise regression [18], detrending method [2,19–23], sensitivity coefficient method and differential method [1,3,14,24,25]. As the aforementioned methods, the differential method can effectively quantify the actual contributions of climate factors to ET_0 trends; therefore, it has been successfully applied in earlier studies.

In recent decades, most scholars have quantified the contributions of meteorological factors to ET_0 trends worldwide, such as China [26–31], Slovenia [16], Spain [32], Iran [33], Bangladesh [34], etc. However, the dominant factors of ET_0 may shift under the changing climate [14,35]. Li et al. [36] pointed out that pan evaporation exhibited a distinct downward trend before 1993 and then reversed in Northwest China. Similarly, Han et al. [35] found a downward trend of ET_0 before 1991 and an upward trend after in the Jing-Jin-Ji region of North China, and the dominant factor contributing to ET_0 shifted from wind speed to mean temperature. Wang et al. [14] revealed that the increasing ET_0 trend after the 1990s over China could be attributed to the increasing air temperature, and the most sensitive factor to ET_0 was specific humidity. However, in Southwest China, the sunshine duration was the main contributor to ET_0 trends in the growing season from 1961 to 1996, and the relative humidity was the dominant variable for the increasing ET_0. Although research scholars have conducted relevant studies on ET_0 [14,37,38], ET_0 varies significantly among diverse regions and the trends of meteorological factors are essential to analyze the variation of ET_0. Thus, it is necessary to conduct regional studies of ET_0, especially in eastern China, where there is still a certain knowledge gap in the systematic study of ET_0. This work intends to close the knowledge gap in the existing literature. Our study also offers a rational theoretical basis for regional agricultural water management and irrigation planning.

The Yangtze River Delta urban agglomeration is one of the six major urban agglomerations in the world. It is an active economic development region, with the highest degree of openness and the strongest innovation ability in China. In 2019, the State Council of the People's Republic of China (PRC) issued the planning scope of the Yangtze River Delta, which officially extended to all the cities in the four provinces of Jiangsu, Zhejiang, Anhui and Shanghai. Anhui province is adjacent to the Yangtze River Delta and is also one of the four provinces mentioned above to have witnessed rapid economic development over the past few decades. Furthermore, Anhui province is one of the 13 major granary provinces, with a total grain output of 34.15 billion kilograms, ranking sixth in China. Among them, the growth rate of the total grain output ranks first among 13 major grain provinces [39].

Thus, an accurate estimation of ET_0, a precise evaluation of its spatiotemporal distribution characteristics and variation trends, as well as the exploration of its influencing factors have scientific implications for agricultural production planning, water resource management, and ecological protection.

Based on the above discussion, we propose the hypothesis that the ET_0 trends and its dominant factors in Anhui province have changed over the past 59 years. To verify this hypothesis, the goals of this research are (1) to investigate the spatiotemporal characteristics of ET_0 and meteorological factors in Anhui province; (2) to clarify the sensitivities of ET_0 to meteorological factors; (3) to determine the dominant factors of ET_0 trends and their internal mechanisms driving ET_0 variations. The outcomes of this research would enhance our understanding of climate change and provide theoretical support for agricultural production and crop water resource management in similar regions worldwide.

2. Materials and methods

2.1. Study Area

Anhui province (114°54′~119°27′ E and 29°41′~34°38′ N), located in the lower Yangtze River Basin and middle Huai River Basin of eastern China, is a transitional zone between the warm temperate zone and the subtropical zone. North of the Huai River belongs to the warm temperate zone with a subhumid monsoon climate, while the south belongs to the subtropical humid monsoon climate zone. Anhui province has a warm and humid climate with four distinct seasons, and the average annual temperature and precipitation are 14~17 °C and 800~1600 mm, respectively. The precipitation is characterized by more south and less north, more mountains and fewer plains and hills. The summer precipitation is abundant, accounting for 40~60% of the annual precipitation. The total area of the province is 139,600 km^2, accounting for about 1.45% of the land area and ranking third in eastern China, as well as twenty-second in China [40]. The terrain in the study area is higher in the south and lower in the north. The southern region is mainly hills and mountains, while the northern is principally plain land (Figure 1a). The Yangtze River and Huai River run through Anhui province for 416 km and 430 km, respectively, dividing the province into three natural regions, namely, the Huaibei Plain, the Jianghuai Hills and southern Anhui mountains. The primary land use type is croplands, with a proportion of approximately 58% of the province's area, followed by grasslands, forests, etc. (Figure 1b).

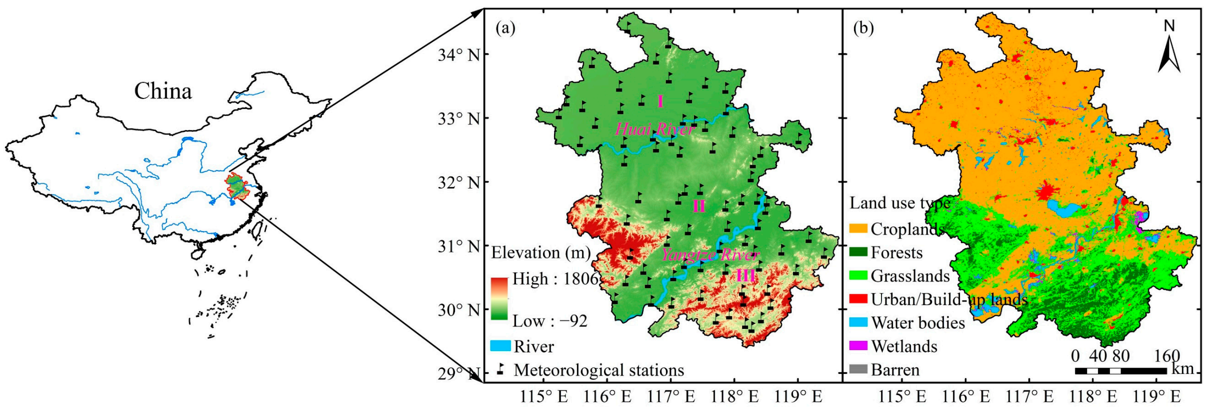

Figure 1. Location, elevation (**a**) and land use type (**b**) of Anhui province in China. **Note:** The Huai River and Yangtze River divide the Anhui province into three regions, namely, Regions I, II and III (**a**). The land use type dataset adopted here was MCD12Q1 of MODIS product in 2014, with the spatial resolution of 500 m × 500 m (**b**).

2.2. Data Sources

The meteorological datasets adopted here were the routine meteorological observation data from 77 weather stations in Anhui province during 1961–2019, which were provided by the China Integrated Meteorological Information Sharing System (CIMISS) of the China

Meteorological Administration (CMA), including daily average temperature (T_a, °C), maximum and minimum temperature (T_{max} and T_{min}, °C), relative humidity (RH, %), sunshine duration (SD, h) and wind speed at 10 m height (u_{10}, $m \cdot s^{-1}$). Quality control of the datasets was already conducted by the National Meteorological Information Center (NMIC) of CMA. In addition, the whole year was divided into five study periods, namely, the growing season (April to October), spring (March to May), summer (June to August), autumn (September to November) and winter (December to February of next year).

2.3. ET_0 Calculation Procedure

The PMF-56 model recommended by the FAO was employed to calculate the ET_0 in this research [5], which is an international accepted method for calculating ET_0. The specific Equation (1) was as follows:

$$ET_0 = \frac{0.408\Delta(R_n - G) + \gamma\frac{900}{T_a+273}u_2(e_s - e_a)}{\Delta + \gamma(1 + 0.34u_2)} \tag{1}$$

where ET_0 refers to the daily reference evapotranspiration ($mm \cdot d^{-1}$), Δ refers to the slope of the curve of the saturation vapor pressure at air temperature T_a ($kPa \cdot °C^{-1}$), R_n refers to the net radiation ($MJ \cdot m^{-2} \cdot d^{-1}$), G refers to the soil heat flux density ($MJ \cdot m^{-2} \cdot d^{-1}$), γ refers to the psychrometric constant ($kPa \cdot °C^{-1}$), T_a refers to the daily air temperature at 2 m height (°C), u_2 refers to the wind speed at a height of 2 m ($m \cdot s^{-1}$) and e_s and e_a refer to the saturation vapor pressure and actual vapor pressure, respectively (kPa).

Due to the missing observation data of solar radiation (R_s, $MJ \cdot m^{-2} \cdot d^{-1}$), Angstrom formula [41] was adopted in this work to estimate R_s through SD data. The detailed Equation (2) was as follows:

$$R_s = \left(a_s + b_s\frac{SD}{SD_{max}}\right)R_a \tag{2}$$

where R_s and R_a denote total daily solar radiation and extraterrestrial radiation, respectively ($MJ \cdot m^{-2} \cdot d^{-1}$), SD and SD_{max} denote daily sunshine duration and maximum possible sunshine duration, respectively (h), and a_s and b_s are regression coefficients, according to the research of Chen et al. [42], with the values of 0.19 and 0.53, respectively.

Meanwhile, while lacking the SD data, the radiation formula put forward by Hargreaves et al. [43] was adopted in this study to calculate R_s through T_{max} and T_{min}; the specific Equation (3) was as follows:

$$R_s = k_{RS} \times \sqrt{(T_{max} - T_{min})} \times R_a \tag{3}$$

where k_{RS} denotes empirical coefficient, and the value in the inland area was usually 0.16 [43–45]. Moreover, the performance of this method was verified in our earlier research [1].

Then, the R_n could be calculated in the following Equations (4)–(6):

$$R_n = R_{ns} - R_{nl} \tag{4}$$

$$R_{ns} = (1 - \alpha)R_s \tag{5}$$

$$R_{nl} = \sigma\left(\frac{T^4_{max,K} + T^4_{min,K}}{2}\right)(0.34 - 0.14\sqrt{e_a})\left(1.35\frac{R_s}{R_{s0}} - 0.35\right) \tag{6}$$

where R_{ns} and R_{nl} are the incoming net short wave radiation and the outgoing net long wave radiation, respectively ($MJ \cdot m^{-2} \cdot d^{-1}$), α is the reference crop albedo (with value of 0.23), σ is the Stephen Boltzmann's constant (4.903×10^{-9} $MJ \cdot K^{-4} \cdot m^{-2} \cdot d^{-1}$), $T_{max,K}$ and $T_{min,K}$ are the maximum and minimum absolute temperature within 24 h (K = °C + 273.16) and R_{s0} is the clear sky radiation ($MJ \cdot m^{-2} \cdot d^{-1}$); for the specific calculation procedure, please refer to work of Allen et al. [5].

As the routine observation data adopted in this study only included u_{10}, in order to obtain the u_2 and the convenience of calculation, our work adopted the wind speed conversion Equation (7) proposed by Allen et al. [5]:

$$u_2 = u_z \frac{4.87}{\ln(67.8z - 5.42)} \tag{7}$$

where u_2 denotes the wind speed with the height of 2 m above the ground plane ($m \cdot s^{-1}$).

In addition, detailed calculations using Equations (8)–(12) of Δ, γ, e_s and e_a were as follows:

$$\Delta = \frac{4098 \times \left[0.6108 \exp\left(\frac{17.27T_a}{T_a + 237.3}\right)\right]}{(T_a + 237.3)^2} \tag{8}$$

$$\gamma = \frac{0.00163P}{\lambda} \tag{9}$$

$$P = 101.3\left(\frac{273 + T_a - 0.0065h}{273 + T_a}\right)^{5.26} \tag{10}$$

$$e_s = 0.6108 \exp\left(\frac{17.27T_a}{T_a + 237.3}\right) \tag{11}$$

$$e_a = e_s \times RH \tag{12}$$

where λ is the latent heat of vaporization with the value of 2.45 ($MJ \cdot kg^{-1}$), P is the atmospheric pressure (kPa) and h is the elevation above the sea level (m).

2.4. Sensitivity Coefficient

The differential equation method developed by McCuen [46] was adopted to calculate the sensitivities of ET_0 to meteorological factors in the following Equation (13):

$$S(v_i) = \lim_{\Delta v_i \to 0}\left(\frac{\Delta ET_0/ET_0}{\Delta v_i/v_i}\right) = \frac{\partial ET_0}{\partial v_i} \times \frac{v_i}{ET_0} \tag{13}$$

where $S(v_i)$ denotes the sensitivity of ET_0 to meteorological factor (v_i), the positive (negative) sensitivity represents the ET_0 increases (decreases) with v_i and the absolute value of $S(v_i)$ denotes the influence of v_i to ET_0. For the detailed calculation processes, please refer to work of Chu et al. [2].

2.5. Contributions of Meteorological Factors to ET_0

As shown in Formula (1), the ET_0 is a function of meteorological factors. Therefore, the T_a, RH, u_2 and R_n were selected as four main meteorological factors affecting ET_0. Moreover, this study employed the differential equation method to assess the contribution of four main meteorological factors to ET_0 based on PMF-56 model. Precise Equation (14) showed as follows:

$$\frac{dET_0}{dt} = \frac{\partial ET_0}{\partial T_a}\frac{dT_a}{dt} + \frac{\partial ET_0}{\partial RH}\frac{dRH}{dt} + \frac{\partial ET_0}{\partial u_2}\frac{du_2}{dt} + \frac{\partial ET_0}{\partial R_n}\frac{dR_n}{dt} + \varepsilon \tag{14}$$

Equation (14) can be abbreviated to the below Equation (15):

$$C\_ET_0 = C(T_a) + C(RH) + C(u_2) + C(R_n) + \varepsilon \tag{15}$$

where C_ET_0 denotes the ET_0 trend, $C(T_a)$, $C(RH)$, $C(u_2)$ and $C(R_n)$ refer to the contribution of T_a, RH, u_2 and R_n to ET_0, respectively, and ε indicates the deviation between C_ET_0 and ET_0 calculated by using Theil–Sen estimator (T_ET_0). The contribution of each meteorological factor to ET_0 could be computed by multiplying the result of Equation (13), the trend of each meteorological factor during the study period and the length of the corresponding study period (i.e., 365 or 366 days for the annual calculation, 214 days for growing season, 92 days for both spring and summer, 91 days for autumn, 90 or 91 days for winter) [1,3].

2.6. Trend Analysis

The Mann–Kendall (M–K) test was recommended for hydrometeorological time series data analysis [47–49]. Thus, it was adopted here to estimate trends of ET_0 and the four main meteorological factors [3]. The null hypothesis H_0 was that in a series of data (x_i, i = 1, 2, . . . , n), x_i was independent and evenly distributed. The alternative hypothesis H_1 was that a monotonic tendency consisted of X. The statistical S and standardized test statistics Z were calculated in the following Equations (16) and (17):

$$S = \sum_{i=1}^{n-1} \sum_{j=i+1}^{n} \operatorname{sgn}(x_j - x_i) \tag{16}$$

$$\operatorname{sgn}(x_j - x_i) = \begin{cases} +1 \text{if } (x_j - x_i) > 0 \\ 0 \text{if } (x_j - x_i) = 0 \\ -1 \text{if } (x_j - x_i) < 0 \end{cases} \tag{17}$$

where x_i and x_j are the value of year i and j, respectively, and n is the data length. The S obeyed normal distributions ($n \geq 8$), the calculation of average value E(S) and variance Var(S) were given below in Equations (18)–(20):

$$E(S) = 0 \tag{18}$$

$$Var(S) = \frac{1}{18}\left[n(n-1)(2n+5) - \sum_{p=1}^{q} t_p(t_p-1)(2t_p+5)\right] \tag{19}$$

where q refers to same group number and t_p represents to the value in pth step.

$$Z = \begin{cases} \frac{S-1}{\sqrt{Vas(S)}} & \text{if } S > 0 \\ 0 & \text{if } S = 0 \\ \frac{S+1}{\sqrt{Vas(S)}} & \text{if } S < 0 \end{cases} \tag{20}$$

in which Z is the change trend of time series' data and Z > 0 (Z < 0) denotes the increasing (decreasing) trend. If $|Z| > Z_{(1-\alpha/2)}$, then the hypothesis was rejected and the time series data showed a significant changing trend. Moreover, $Z_{(1-\alpha/2)}$ was the standard normal deviation in the standard normal distribution chart. When the α = 5% and α = 1% were the significant levels, the $Z_{(1-\alpha/2)}$ values were 1.96 and 2.58, respectively.

The Theil–Sen estimator was used to determine the magnitude of the variation trends of ET_0 and meteorological factors [50,51]. Detailed calculation Equation (21) was as follows:

$$\beta = \operatorname{Median}\left(\frac{x_j - x_i}{j-i}\right), \forall 1 < i < j \tag{21}$$

where β is the calculated slope of data series; x_i and x_j represent the sequence data corresponding to time i and j, respectively; the positive (negative) β indicates the increasing (decreasing) trend. Spatial distribution map was prepared by inverse distance weighting (IDW) method within ArcGIS platform (version 10.2).

3. Results

3.1. Spatiotemporal Variations of ET_0

3.1.1. Temporal Scale

As shown in Figure 2, the ET_0 exhibited a significant decreasing trend before 1990 (-3.89 mm·a^{-2}) and then increased slowly (0.62 mm·a^{-2}) throughout the entire region. In subregions, the ET_0 presented significant decreasing trends before 1990, and the decrease magnitudes ranked in the order: Region I > Region II > Region III. After 1990, the ET_0 showed a slowly decreasing trend in Region I, while it exhibited slow increasing trends in other regions, being especially higher in Region III. Because of the definition of the World Meteorological Organization (WMO) of the standard climate standard (i.e., the 30-year average) and the opposite change trend of ET_0 around 1990 in this study, we divided the entire study period into two periods, namely, 1961–1990 and 1991–2019.

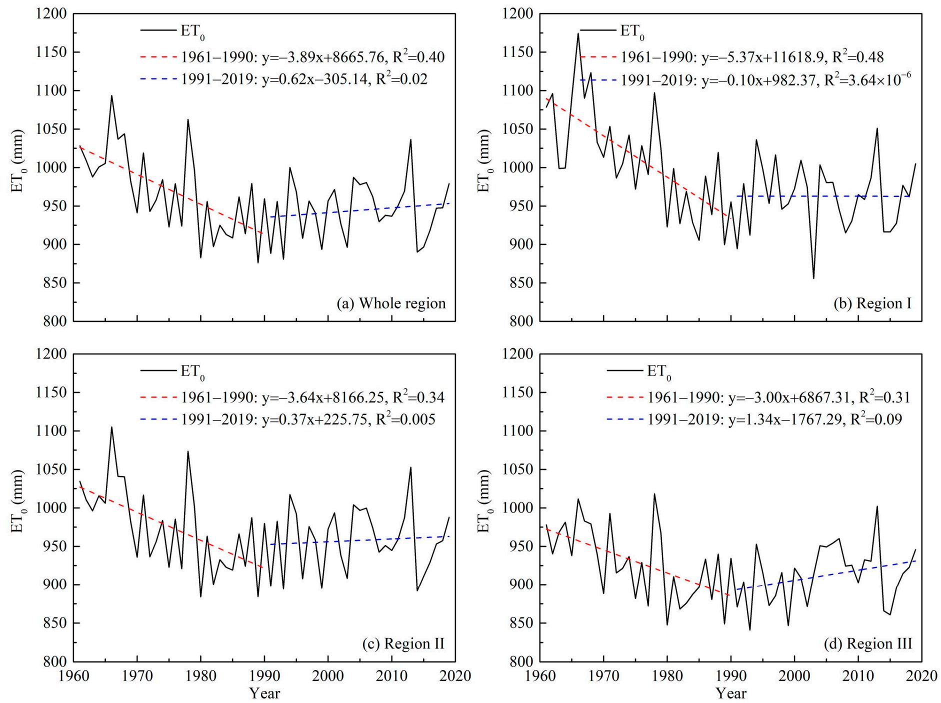

Figure 2. Temporal variations of ET_0 during 1961–2019 in Anhui province (**a**) Whole region, (**b**) Region I, (**c**) Region II, (**d**) Region III.

Detailed temporal trends of ET_0 are also shown in Table 1. Before 1990, the temporal trends of ET_0 on an annual timescale, growing season, and summer were similar. During spring, autumn and winter, the downward trends of ET_0 were not significant in most regions. After 1990, ET_0 exhibited slow upward trends annually, during the growing season, spring and summer, while it showed downward trends during autumn and winter. It is worth noting that only the ET_0 trend in Region III in spring was significant.

Table 1. Temporal trends of ET_0 during 1961–1990 and 1991–2019 in Anhui province.

Time	Region	Annual		Growing Season		Spring		Summer		Autumn		Winter	
		Z	β	Z	β	Z	β	Z	Β	Z	β	Z	β
1961–1990	Whole	−3.53	−3.953 ***	−2.96	−2.861 **	−1.07	−0.474	−2.85	−2.242 **	−1.61	−0.494	−1.64	−0.390
	I	−3.93	−5.254 ***	−3.75	−4.148 ***	−2.14	−1.256 *	−3.78	−3.066 ***	−1.57	−0.450	−1.50	−0.548
	II	−3.25	−3.567 **	−2.78	−2.672 **	−0.82	−0.362	−2.93	−2.233 **	−1.68	−0.499	−1.53	−0.343
	III	−2.96	−3.188 **	−2.32	−2.363 *	−1.03	−0.258	−1.96	−1.748 *	−1.93	−0.554	−1.89	−0.326
1991–2019	Whole	0.62	0.552	0.54	0.364	1.26	0.809	0.88	0.594	−1.44	−0.478	−0.58	−0.096
	I	−0.02	−0.059	−0.21	−0.286	0.73	0.364	0.06	0.046	−1.22	−0.555	−0.66	−0.198
	II	0.21	0.199	0.13	0.075	1.26	0.850	0.96	0.619	−1.67	−0.541	−0.88	−0.155
	III	1.59	1.339	1.26	1.120	2.04	1.029 *	0.73	0.551	−0.51	−0.139	−0.36	−0.091

Note: Z indicates the M–K test statistic; β is the estimated ET_0 slope, $\beta > 0$ ($\beta < 0$) denotes increasing (decreasing) trend; *, ** and *** denote the significance level of 0.05, 0.01 and 0.001, respectively.

3.1.2. Spatial Scale

As shown in Figure 3, the spatial distribution of ET_0 during 1961–1990 and 1991–2019 was basically consistent. The ET_0 was higher in the north and lower in the south annually, during the growing season, spring and summer. However, the ET_0 was higher in the southwest of Regions II and III in both autumn and winter. Before 1990, ET_0 annually, during the growing season and summer showed a significant decreasing trend in most regions. After 1990, the ET_0 in Region III showed a significant increasing trend annually, during the growing season and spring. Moreover, the ET_0 in Region II also exhibited a significant increasing trend in spring. These phenomena are echoed in Table 1.

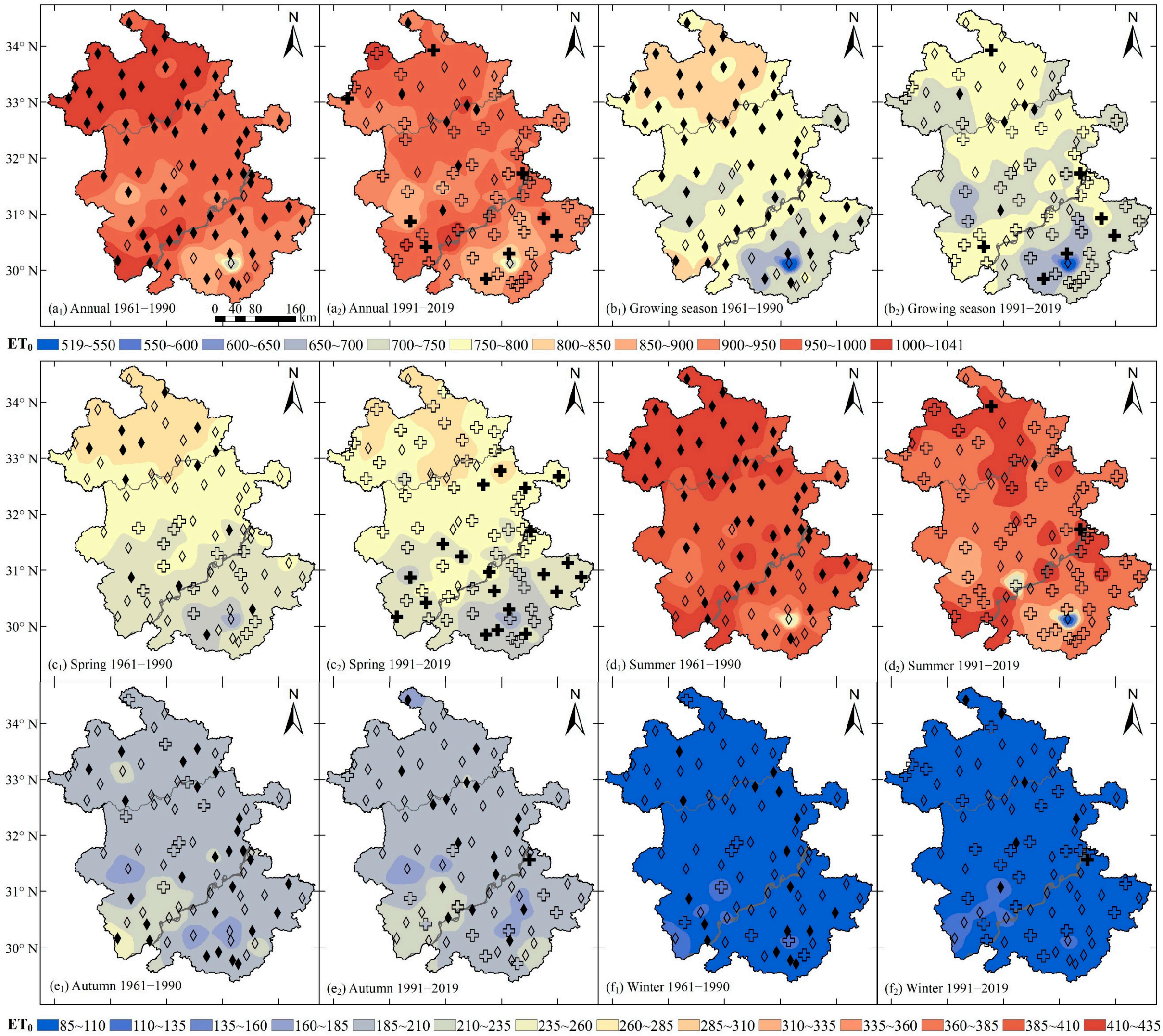

Figure 3. Spatial trends of ET_0 during 1961–1990 and 1991–2019 in Anhui province. **Note:** Solid (hollow) rhombus and plus sign indicate significant (insignificant) downward and upward trends, respectively.

3.2. Spatiotemporal Variations of Meteorological Factors

To evaluate the impact of meteorological factors on ET_0, we analyzed the change trends of meteorological factors. As shown in Figure 4, T_a decreased significantly at the rate of $-0.021\ ^{\circ}C \cdot a^{-1}$ before 1990, and then increased significantly with the rate of $0.034\ ^{\circ}C \cdot a^{-1}$ (Figure 4a). RH first increased at the rate of 0.071 a^{-1} before 1990, and then decreased slightly at the rate of 0.070 a^{-1} (Figure 4b). u_2 declined significantly with the rate of $-0.020\ m \cdot s^{-1}$ before 1990, and then slowed down to $-0.006\ m \cdot s^{-1}$ (Figure 4c). Similar to

u_2, R_n also declined significantly with the rate of -0.017 MJ·m^{-2}·d^{-1} before 1990, and then slowed down to -0.004 MJ·m^{-2}·d^{-1} insignificantly (Figure 4d).

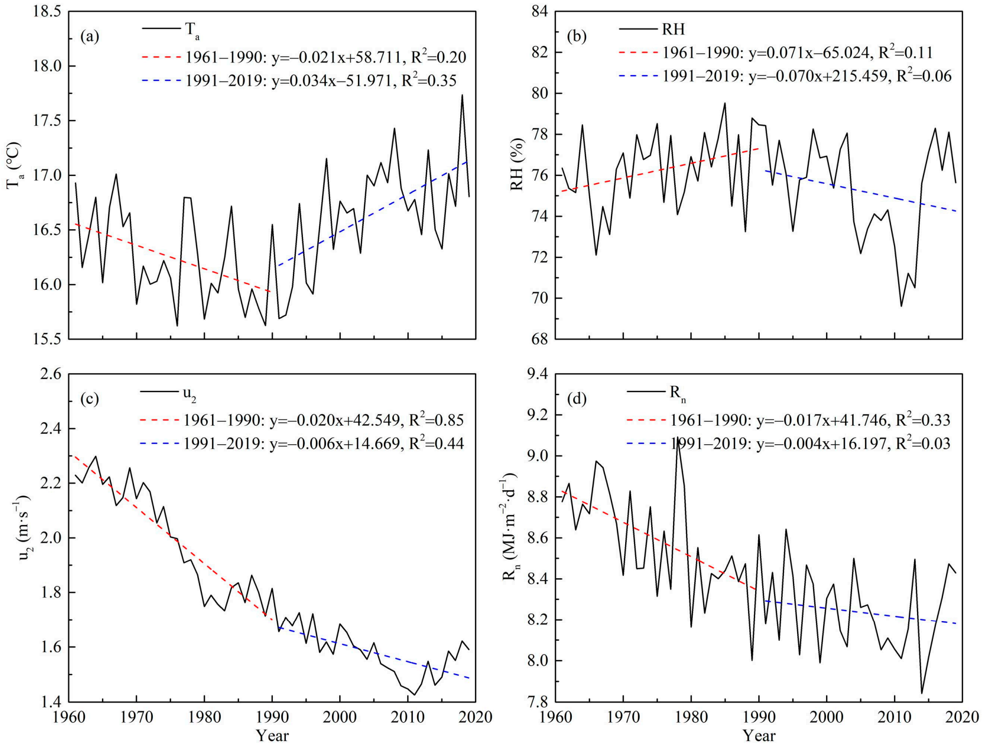

Figure 4. Temporal variations of meteorological factors (**a**) T_a, (**b**) RH, (**c**) u_2, (**d**) R_n during 1961–2019 in Anhui province.

From Table 2, T_a exhibited significant decreasing trends in the entire region and each subregion on an annual timescale and in Regions I and II in summer, while showing insignificant decreasing trends in other regions and timescales during 1961–1990. During 1991–2019, T_a showed increasing trends in all regions and study periods, with significant trends exhibited annually, during the growing season, spring, summer and autumn in most regions. RH showed increasing trends before 1990 in most regions, while it showed decreasing trends after 1990, except in autumn. u_2 presented significant decreasing trends in most regions during the two time periods, except in Region III after 1990, which exhibited slightly increasing trends. R_n decreased significantly annually, during the growing season, summer and winter, while insignificantly in other periods before 1990. Then, R_n decreased slowly in most regions and study periods, except in spring, which increased slowly after 1990.

3.3. Sensitivity of Meteorological Factors to ET_0

3.3.1. Temporal Variation Characteristics

The daily sensitivity coefficient of each meteorological factor to ET_0 is shown in Figure 5. As seen from Figure 5, the daily sensitivity coefficient of T_a, RH and R_n (i.e., $S(T_a)$, S(RH) and $S(R_n)$) first increased and then decreased, while the daily sensitivity coefficient of u_2 ($S(u_2)$) showed a gradual changing trend, going downward first and then upward. The magnitude of these four meteorological factors was ranked as follows: S(RH) > $S(R_n)$ > $S(T_a)$ > $S(u_2)$. In contrast to $S(T_a)$, $S(u_2)$ and $S(R_n)$, S(RH) was negative.

Table 2. Temporal trends of meteorological factors during 1961–1990 and 1991–2019 in Anhui province.

Meteorological Factor	Time	Region	Annual		Growing Season		Spring		Summer		Autumn		Winter	
			Z	β	Z	β	Z	β	Z	β	Z	β	Z	β
T_a	1961–1990	Whole	−2.57	−0.022 *	−1.64	−0.011	−0.86	−0.007	−1.82	−0.035	−0.54	−0.007	−0.75	−0.010
		I	−2.36	−0.029 *	−1.86	−0.017	−0.75	−0.009	−2.25	−0.039 *	−0.04	−0.001	−0.54	−0.004
		II	−2.71	−0.021 **	−1.57	−0.012	−0.57	−0.007	−2.00	−0.036 *	−0.57	−0.008	−1.14	−0.012
		III	−2.50	−0.020 *	−1.25	−0.009	−0.96	−0.013	−1.32	−0.019	−0.61	−0.009	−0.61	−0.013
	1991–2019	Whole	2.91	0.036 **	2.46	0.032 *	3.28	0.059 **	2.12	0.030 *	2.76	0.031 **	0.84	0.009
		I	2.76	0.037 **	2.12	0.026 *	3.06	0.053 **	1.52	0.026	2.31	0.026 *	1.07	0.015
		II	2.87	0.035 **	2.27	0.028 *	3.10	0.062 **	1.97	0.02 9 *	2.08	0.026 *	0.73	0.011
		III	3.21	0.038 **	2.79	0.035 **	3.17	0.054 **	1.78	0.030	2.98	0.042 **	0.69	0.011
RH	1961–1990	Whole	1.78	0.0009	1.50	0.0008	0.14	0.0002	2.78	0.0012 **	0.36	0.0002	0.61	0.0008
		I	2.36	0.0016 *	1.86	0.0014	0.89	0.0011	2.93	0.0021 **	0.43	0.0005	0.54	0.0012
		II	1.32	0.0006	1.21	0.0007	−0.11	−0.0001	2.46	0.0012 *	0.21	0.0001	0.39	0.0004
		III	1.50	0.0005	1.00	0.0004	−0.18	−0.00004	1.46	0.0009	0.61	0.0004	0.89	0.0006
	1991–2019	Whole	−1.07	−0.0008	−1.37	−0.0009	−1.29	−0.0016	−1.29	−0.0009	0.66	0.0007	−0.06	−0.0001
		I	−0.88	−0.0005	−0.84	−0.0007	−0.47	−0.0009	−0.99	−0.0006	0.47	0.0007	−0.09	−0.0001
		II	−1.18	−0.0008	−1.18	−0.0007	−1.48	−0.0019	−0.88	−0.0007	1.03	0.0009	−0.36	−0.0003
		III	−0.88	−0.0005	−1.41	−0.0010	−1.67	−0.0016	−1.22	−0.0008	0.69	0.0006	0.43	0.0004
u_2	1961–1990	Whole	−5.67	−0.021 ***	−5.28	−0.019 ***	−5.32	−0.024 ***	−4.78	−0.014 ***	−5.32	−0.023 ***	−5.03	−0.023 ***
		I	−5.53	−0.025 ***	−5.03	−0.023 ***	−4.92	−0.029 ***	−4.53	−0.020 ***	−5.25	−0.027 ***	−5.35	−0.031 ***
		II	−5.46	−0.019 ***	−4.78	−0.017 ***	−5.00	−0.023 ***	−4.32	−0.012 ***	−4.89	−0.023 ***	−4.82	−0.021 ***
		III	−5.71	−0.018 ***	−5.07	−0.016 ***	−5.46	−0.022 ***	−3.71	−0.012 ***	−5.07	−0.019 ***	−5.57	−0.020 ***
	1991–2019	Whole	−3.55	−0.008 ***	−3.25	−0.007 **	−4.60	−0.009 ***	−2.38	−0.005 *	−1.97	−0.005 *	−2.04	−0.004 *
		I	−3.43	−0.011 ***	−3.28	−0.010 **	−4.15	−0.014 ***	−2.91	−0.010 **	−2.91	−0.009 **	−1.82	−0.006
		II	−4.18	−0.011 ***	−3.62	−0.011 ***	−4.75	−0.013 ***	−3.36	−0.010 ***	−2.53	−0.009 *	−2.68	−0.007 **
		III	1.03	0.001	1.48	0.003	0.47	0.001	1.03	0.003	1.52	0.003	0.58	0.001
R_n	1961–1990	Whole	−3.00	−0.017 **	−2.36	−0.020 *	−0.71	−0.007	−2.57	−0.047 *	−1.14	−0.006	−2.53	−0.010 *
		I	−3.03	−0.016 **	−2.50	−0.021 *	−1.00	−0.010	−3.32	−0.053 ***	−0.75	−0.003	−3.07	−0.009 **
		II	−2.71	−0.018 **	−2.28	−0.021 *	−0.75	−0.008	−2.60	−0.048 **	−1.00	−0.007	−2.60	−0.010 **
		III	−2.78	−0.016 **	−2.32	−0.019 *	−0.61	−0.003	−1.96	−0.040 *	−1.75	−0.012	−2.28	−0.008 *
	1991–2019	Whole	−0.92	−0.005	−0.69	−0.008	0.84	0.008	−0.51	−0.010	−2.57	−0.017 *	−2.46	−0.008 *
		I	−0.66	−0.004	−0.92	−0.007	0.58	0.003	−0.62	−0.011	−1.89	−0.012	−2.57	−0.009 *
		II	−0.96	−0.006	−0.99	−0.011	0.66	0.006	−0.54	−0.009	−2.49	−0.017 *	−2.31	−0.008 *
		III	−0.32	−0.003	−0.06	−0.001	1.63	0.013	0.28	0.005	−2.49	−0.016 *	−1.67	−0.006

Note: Z indicates the M–K test statistic; β refers to the estimated slope of meteorological factor, β > 0 (β < 0) denotes the increasing (decreasing) trend; *, ** and *** indicate significance level of 0.05, 0.01 and 0.001, respectively.

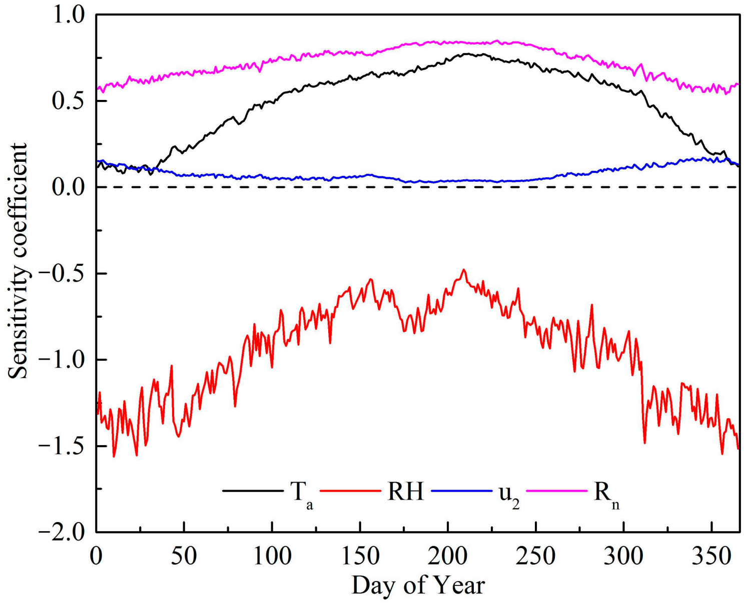

Figure 5. Changes of daily sensitivity coefficients of meteorological factors to ET_0 for the whole period.

Table 3 presents the seasonal variation of the sensitivities of meteorological factors to ET_0. The general change trends of sensitivity coefficients in the seasonal timescale were consistent with those in the daily timescale. During 1961–1990, the ET_0 was most sensitive to RH annually, during the growing season, spring, autumn and winter, and the sensitivity magnitude of four meteorological factors was ranked as follows: S(RH) > S(R_n) > S(T_a) > S(u_2). However, the ET_0 was most sensitive to Rn in summer, followed by T_a, RH and u_2 in all regions. Furthermore, the ET_0 was most sensitive to R_n in the growing season, followed by RH, T_a and u_2 in Region III. In contrast to that during 1961–1990, the ET_0 was most sensitive to R_n in the growing season, followed by RH, T_a and u_2 during 1991–2019. Moreover, R_n was also the most sensitive factor in spring in Region III. The differences between these two time periods were not distinct.

Table 3. Sensitivities of ET_0 to meteorological factors during 1961–1990 and 1991–2019.

Region	Season	1961–1990				1991–2019			
		S(T_a)	S(RH)	S(u_2)	S(R_n)	S(T_a)	S(RH)	S(u_2)	S(R_n)
Whole	Annual	0.489	**−1.033**	0.074	0.709	0.492	**−0.886**	0.082	0.731
	Growing season	0.660	**−0.824**	0.049	0.778	0.641	−0.683	0.060	**0.791**
	Spring	0.499	**−0.971**	0.049	0.724	0.507	**−0.753**	0.066	0.740
	Summer	0.728	−0.691	0.037	**0.817**	0.692	−0.628	0.044	**0.830**
	Autumn	0.578	**−1.078**	0.090	0.707	0.575	**−0.906**	0.098	0.726
	Winter	0.152	**−1.398**	0.119	0.588	0.194	**−1.253**	0.121	0.628
I	Annual	0.474	**−1.024**	0.102	0.652	0.477	**−0.871**	0.104	0.690
	Growing season	0.666	**−0.817**	0.070	0.737	0.643	−0.664	0.072	**0.770**
	Spring	0.505	**−0.903**	0.079	0.658	0.511	**−0.713**	0.086	0.698
	Summer	0.736	−0.713	0.054	**0.783**	0.696	−0.618	0.053	**0.814**
	Autumn	0.565	**−1.095**	0.115	0.660	0.559	**−0.904**	0.119	0.692
	Winter	0.090	**−1.393**	0.159	0.507	0.144	**−1.243**	0.160	0.556
II	Annual	0.499	**−1.080**	0.075	0.701	0.501	**−0.920**	0.086	0.720
	Growing season	0.669	**−0.861**	0.051	0.771	0.650	−0.713	0.064	**0.780**

Table 3. *Cont.*

Region	Season	1961–1990				1991–2019			
		S(T_a)	S(RH)	S(u_2)	S(R_n)	S(T_a)	S(RH)	S(u_2)	S(R_n)
III	Spring	0.507	**−1.019**	0.048	0.718	0.516	**−0.777**	0.071	0.728
	Summer	0.737	−0.720	0.038	**0.813**	0.701	−0.657	0.046	**0.823**
	Autumn	0.589	**−1.123**	0.095	0.694	0.584	**−0.943**	0.104	0.713
	Winter	0.164	**−1.464**	0.120	0.580	0.203	**−1.297**	0.125	0.616
	Annual	0.483	**−0.954**	0.052	0.763	0.487	**−0.838**	0.060	0.777
	Growing season	0.640	−0.758	0.033	**0.820**	0.626	−0.644	0.045	**0.823**
	Spring	0.482	**−0.930**	0.029	0.778	0.491	−0.736	0.046	**0.785**
	Summer	0.707	−0.619	0.025	**0.849**	0.676	−0.581	0.033	**0.854**
	Autumn	0.568	**−0.979**	0.065	0.763	0.570	**−0.846**	0.074	0.773
	Winter	0.176	**−1.288**	0.090	0.660	0.211	**−1.185**	0.088	0.696

Note: The bold font represents the most sensitive factor.

Figure 6 shows the annual sensitivity coefficients of meteorological factors to ET_0. S(T_a) exhibited a slow downward trend during the whole study period, decreased before 1990 and then increased. S(RH) and S(R_n) both presented evident increasing trends in the past 59 years, especially during 1961–1990. Because the S(RH) was negative, as far as the magnitude was concerned, the sensitivity of RH decreased generally. S(u_2) was similar to S(T_a), while it increased more obviously after 1990.

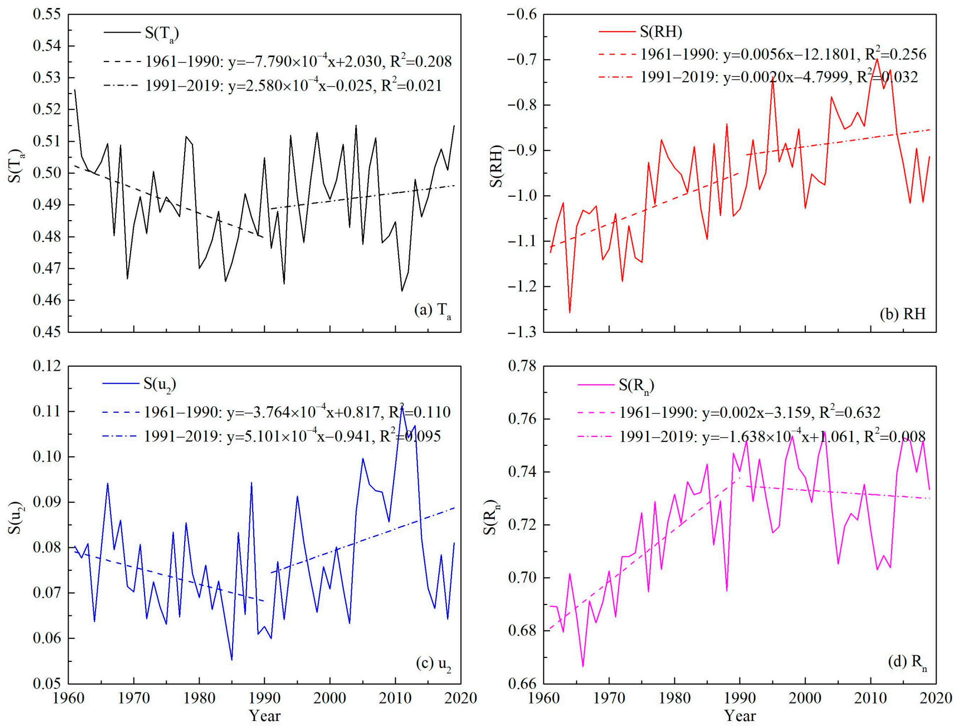

Figure 6. Changes of annual sensitivity coefficients of meteorological factors (**a**) T_a, (**b**) RH, (**c**) u_2, (**d**) R_n to ET_0.

3.3.2. Spatial Variation Characteristics

In order to illuminate the sensitivity coefficients of ET_0 to meteorological factors, the spatial distribution of annual mean sensitivity coefficients is displayed in Figure 7. As shown in Figure 7, S(T_a) was higher in Region II, especially along the Yangtze River, than in the north of Region I, west of Region II and south of Region III. The spatial distribution of S(RH) was similar to that of S(T_a), while the highest value was located in the central Region III (namely, the Huangshan station). S(u_2) was comparatively higher in the north and lower in the south. The $S(u_2)$ in the west of Region II was lower than in surrounding regions. Contrary to the spatial distribution of $S(T_a)$ and $S(RH)$, the higher values of $S(R_n)$ were mainly located in the west of Region II and most areas of Region III.

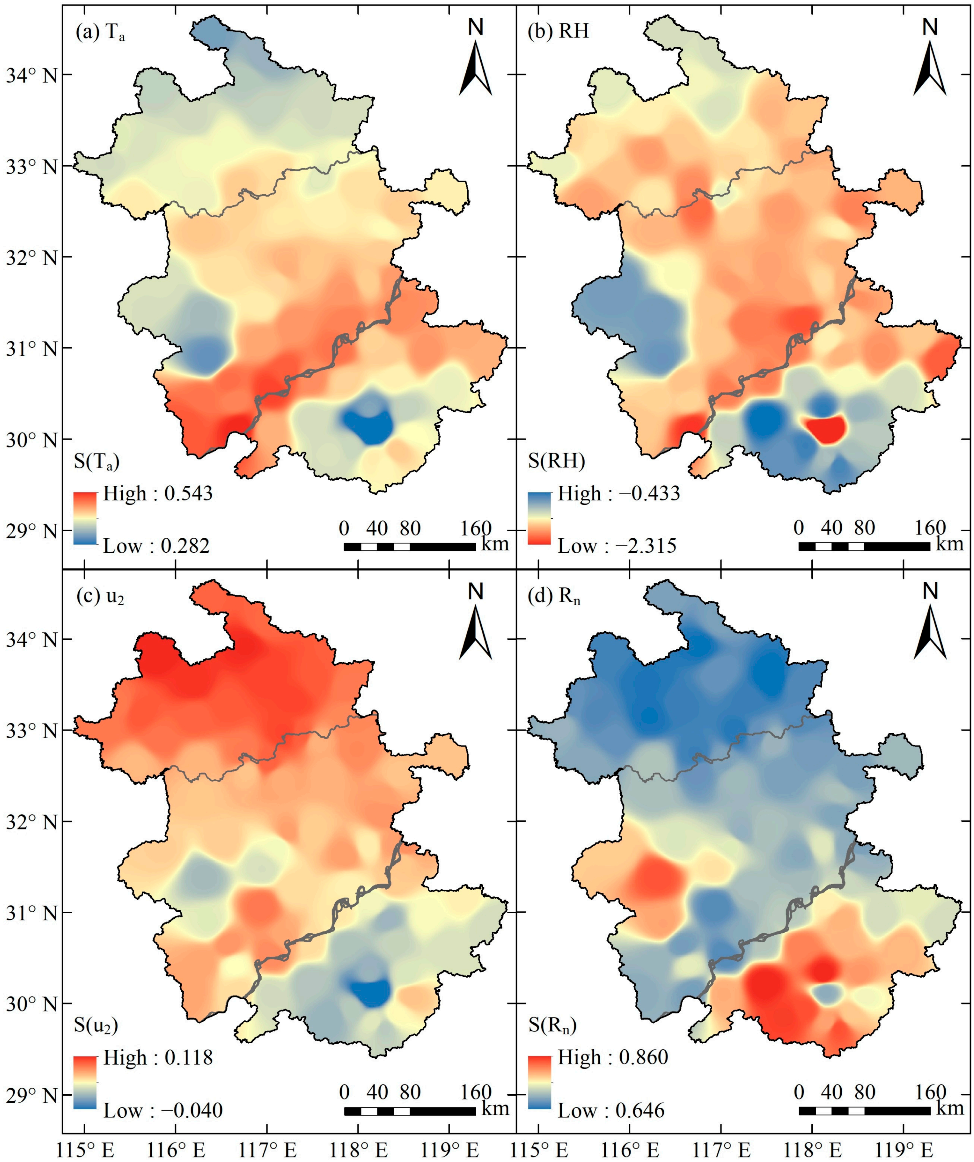

Figure 7. Space distribution of annual mean sensitivity coefficient of ET_0 to meteorological factors (**a**) T_a, (**b**) RH, (**c**) u_2, (**d**) R_n.

3.4. Contribution of Meteorological Factors to ET_0

3.4.1. Validation of Differential Method

To verify the validity of the differential method, we compared the ET_0 trends calculated using a differential method (C_ET_0) and with those, the Sen slope estimator (E_ET_0) in three time periods (during 1961–2019, 1961–1990 and 1991–2019). As shown in Figure 8, the fitting results from the differential method and the Sen slope estimator were all concentrated in a 1:1 line, with an R^2 value generally greater than 0.90. Thus, all the above phenomena indicated that the four selected meteorological factors in this research were reasonable and could be well explained by the contributions to ET_0 trends by employing the differential method.

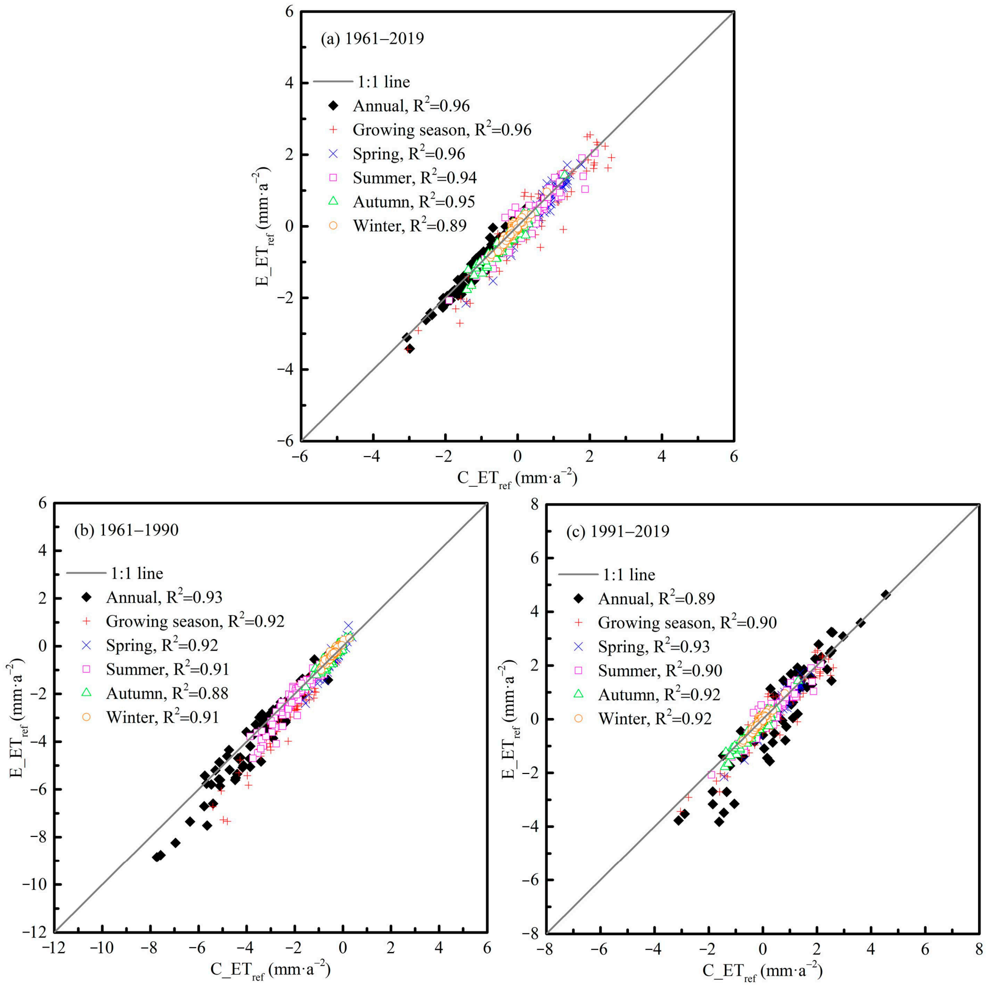

Figure 8. Validation of differential equation method in annual and seasonal timescale during 1961–2019 (**a**), 1961–1990 (**b**) and 1991–2019 (**c**).

3.4.2. Contribution of Meteorological Factors to ET_0

The contribution of meteorological factors to the ET_0 trend during the two study periods is shown in Figure 9. During 1961–1990, all meteorological factors offered negative contributions to ET_0 trends, which ultimately led to decreasing trends for almost all regions and periods (Table 1). Specifically, R_n was the leading factor annually, during the growing season and summer, while u_2 played leading roles in spring, autumn and winter. However, RH was the leading factor in Region I annually and R_n was the leading factor in Region III in autumn. During 1991–2019, T_a and RH showed positive contributions to ET_0 trends for most regions and periods, except for RH in autumn and winter. In contrast, u_2 and R_n devoted negative contributions to ET_0 trends, except for R_n in spring and summer and u_2 in Region III. Concretely, the main reason for changes in the ET_0 was T_a annually, during the growing season, spring and summer, and then R_n in autumn and winter for most regions. Moreover, notably, the contribution magnitude of u_2 to ET_0 trends dropped sharply in Region III for all seasons. Overall, the negative contributions from u_2 and R_n could not offset the positive contributions from T_a and RH, which led to the slow upward ET_0 trends in the entire region, eventually, while the upward trend was higher in Region III. Table 4 and Figures S1 and S2 in the Supplementary Materials provide detailed information and the spatial distribution of dominant factors.

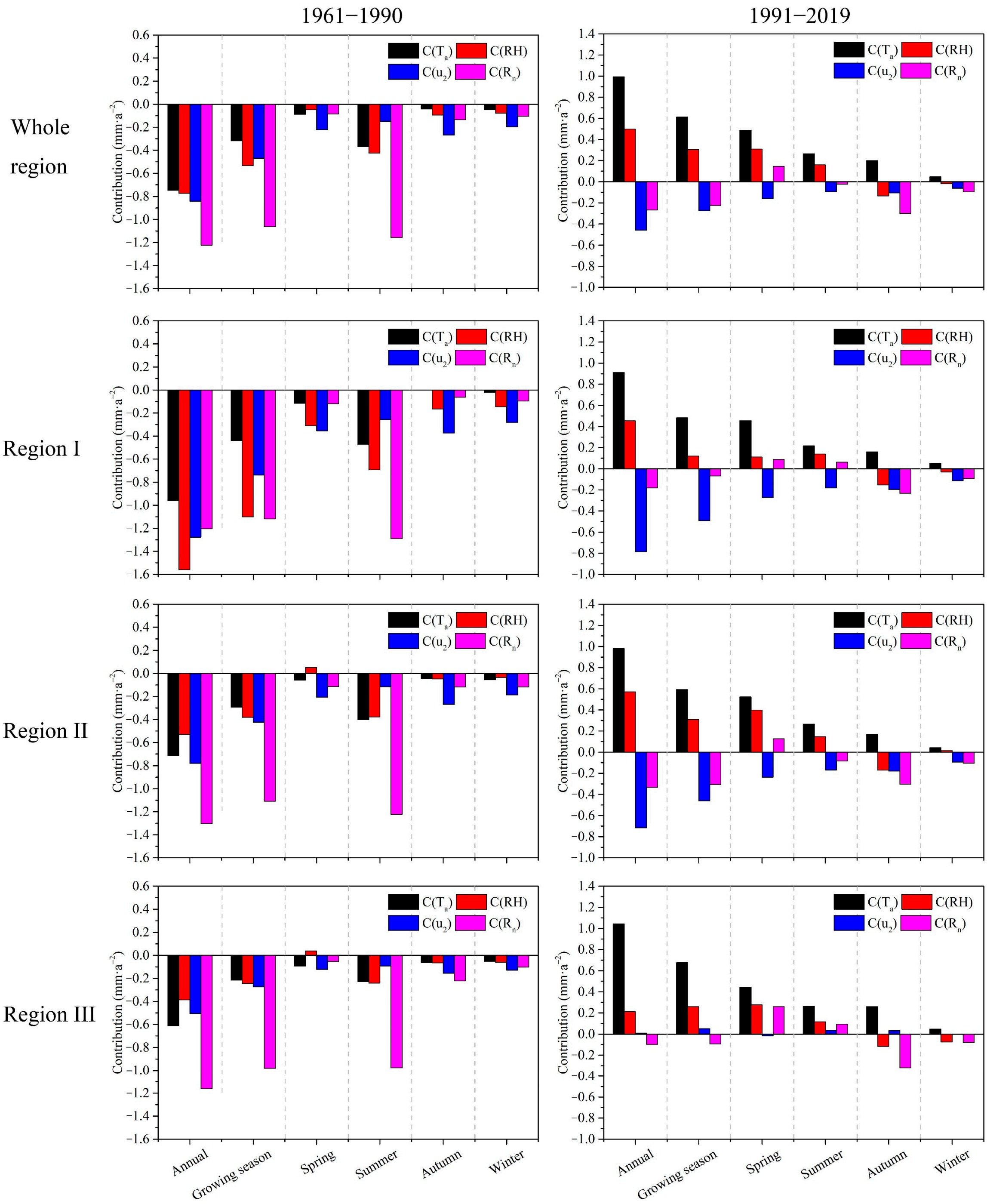

Figure 9. Contributions of meteorological factors to ET_0 trends during 1961–1990 and 1991–2019.

Table 4. Contributions of meteorological factors to ET_0 trends during 1961–1990 and 1991–2019.

Region	Season	1961–1990				1991–2019			
		C(T$_a$)	**C(RH)**	**C(u$_2$)**	**C(R$_n$)**	**C(T$_a$)**	**C(RH)**	**C(u$_2$)**	**C(R$_n$)**
Whole	Annual	−0.746	−0.772	−0.842	**−1.223**	**0.993**	0.499	−0.459	−0.267
	Growing season	−0.317	−0.533	−0.470	**−1.063**	**0.612**	0.304	−0.274	−0.225
	Spring	−0.088	−0.049	**−0.221**	−0.085	**0.486**	0.309	−0.160	0.146
	Summer	−0.368	−0.424	−0.150	**−1.158**	**0.265**	0.159	−0.094	−0.023

Table 4. *Cont.*

Region	Season	1961–1990				1991–2019			
		C(T_a)	C(RH)	C(u_2)	C(R_n)	C(T_a)	C(RH)	C(u_2)	C(R_n)
	Autumn	−0.041	−0.094	**−0.268**	−0.136	0.201	−0.133	−0.105	**−0.300**
	Winter	−0.047	−0.077	**−0.196**	−0.106	0.047	−0.018	−0.061	**−0.095**
I	Annual	−0.959	**−1.560**	−1.277	−1.204	**0.910**	0.454	−0.785	−0.181
	Growing season	−0.438	−1.101	−0.738	**−1.118**	0.483	0.122	**−0.490**	−0.068
	Spring	−0.115	−0.311	**−0.355**	−0.119	**0.455**	0.111	−0.272	0.087
	Summer	−0.471	−0.693	−0.257	**−1.290**	**0.215**	0.140	−0.180	0.062
	Autumn	0.000	−0.164	**−0.374**	−0.062	0.161	−0.152	−0.197	**−0.233**
	Winter	−0.021	−0.145	**−0.282**	−0.096	0.051	−0.030	**−0.113**	−0.093
II	Annual	−0.713	−0.528	−0.781	**−1.304**	**0.980**	0.572	−0.715	−0.333
	Growing season	−0.294	−0.381	−0.424	**−1.110**	**0.592**	0.307	−0.461	−0.306
	Spring	−0.057	0.050	**−0.207**	−0.114	**0.523**	0.399	−0.238	0.126
	Summer	−0.402	−0.378	−0.116	**−1.223**	**0.265**	0.146	−0.170	−0.085
	Autumn	−0.044	−0.048	**−0.268**	−0.118	0.170	−0.170	−0.179	**−0.304**
	Winter	−0.055	−0.034	**−0.187**	−0.117	0.042	0.015	−0.094	**−0.103**
III	Annual	−0.611	−0.387	−0.505	**−1.161**	**1.043**	0.212	0.009	−0.098
	Growing season	−0.216	−0.244	−0.273	**−0.981**	**0.676**	0.260	0.052	−0.095
	Spring	−0.093	0.037	**−0.123**	−0.052	**0.442**	0.277	−0.017	0.260
	Summer	−0.227	−0.240	−0.093	**−0.977**	**0.264**	0.116	0.035	0.094
	Autumn	−0.064	−0.065	−0.156	**−0.222**	0.260	−0.117	0.033	**−0.320**
	Winter	−0.052	−0.060	**−0.129**	−0.102	0.048	−0.074	0.001	**−0.079**

Note: The bold font represents the most dominant factor.

4. Discussion

In this study, T_a exhibited significant decreasing and increasing trends before and after 1990, respectively, which was similar to that in the whole of China [52] and also surrounding regions, such as the Huai River Basin [53] and Jiangsu province [2]. Ding et al. [52] pointed out that the sum of positive radiative forcing generated by greenhouse gases was the cause of climate warming, and that the surface temperature is likely to continue to rise. On the contrary, the RH first increased and then decreased, which may also be explained by the climate warming in this region (namely, the change trends in T_a). Furthermore, the larger vapor pressure deficit (VPD) caused by climate change from 1983 to 2008 [54] could explain the RH changing trends. Here, the changing trend of u_2 was similar to that in mainland China [55]. However, because Region III is mainly a mountainous terrain zone, it was greatly affected by the narrow tube effect, which resulted in a higher wind speed here. These phenomena might be responsible for the relatively lower decreasing trends of u_2 during 1961–1990 and slightly increasing trends during 1991–2019. Moreover, Tao et al. [56] reported that urbanization also had an impact on the annual mean wind speed decline in Anhui province after 2000 and its contribution rate reached 40%, particularly in spring. Meanwhile, the attenuation factor u_2 might suppress the diffusion of aerosols and strengthen the influence of aerosol emissions on solar dimming [57]. In addition, Qian et al. [58] indicated that a fog-like haze caused by increasing air pollution might absorb or reflect the radiation, resulting in a reduction in surface solar radiation. Similar results were also shown by Ma et al. [59], Qi et al. [60] and Tao et al. [61].

This research also revealed that the ET_0 decreased significantly before 1990 and then increased slowly. Similar phenomena occurred in a desertification-prone region of China [62], the Yellow River Basin [31], the Jing-Jin-Ji region of North China [35], Xinjiang province [63] and even mainland China [14,64]. All these changing trends in ET_0 were attributed to changes in meteorological factors before and after the change point in specific regions. Generally, in this research, ET_0 was most sensitive to RH, followed by R_n, T_a and u_2, while the most sensitive factor shifted to R_n in summer, followed by T_a, RH and u_2 for most regions. Similar results could be found in the Huai River Basin [1] and Jiangsu province [2]. However, in other regions of China, Xu et al. [27] pointed out that T_{max} was, generally, the most sensitive factor for ET_0, followed by RH, R_s, T_{min} and u_2 in the Jing River Basin of Northwest China. Wang et al. [65] reported that the ET_0 was more sensitive to T_{max} and SD than RH, u_2 and T_{min} in the three-river headwaters region of the Qinghai–Tibetan Plateau. Li et al. [29] discovered that the RH had the highest sensitivity, followed by T_{max}, u_2, SD and T_{min}. She et al. [31] and Yang et al. [66] both indicated that the ET_0 was the most sensitive to R_s, followed by RH and T_a in parts of the Yellow River Basin. From the previous research above, the difference in sensitivity factors of ET_0 in different regions of China may have been mainly caused by the lower water vapor carried by the wind in dry regions and the higher humidity of the wind flow in humid regions [64]. However, in summer, and even in the growing season of Anhui province, T_a and R_n increased, while the air pressure and RH decreased, which could explain the transition of the most sensitive factor of ET_0 from RH to R_n.

Although ET_0 was most sensitive to RH for most regions, the change rate of RH was relatively small compared to other factors. Before 1990, R_n was the leading factor of ET_0 trends annually, during the growing season and summer, while u_2 was the leading factor in spring, autumn and winter. However, the high contribution of RH to the ET_0 trend in Region I in the annual timescale could be interpreted reasonably by its significant increasing trend (Table 2). During 1991–2019, the leading factor of ET_0 trends changed to T_a annually, during the growing season, spring and summer, then to R_n in autumn and winter for most regions. Similarly, Han et al. [35] reported that a decreasing sunshine duration and wind speed offset the impact of increasing air temperature, resulting in a decrease in ET_0 between 1961 and 1991, while T_a was the most dominant factor contributing to an increase in ET_0 in the Jing-Jin-Ji region between 1992 and 2015. Wang et al. [14] reported that the ET_0 presented a significant increasing trend after the 1990s in China due to the increasing T_a. In this study, we also demonstrated an interesting phenomenon that the significance of climate variables was proportional to their dominance in ET_0 trends. This finding was supported by a similar finding in our previous study on pan evaporation in the Huai River Basin [3]. As shown in Table 2, during 1961–1990, R_n represented significant decreasing trends annually, during the growing season and summer, which may explain its dominant role in the corresponding seasons. Although u_2 always showed significant downward trends in these periods, the magnitude of u_2 trends in spring, autumn and winter was larger than those in other seasons, which might have been responsible for its dominance in corresponding seasons. However, during 1991–2019, T_a presented prominently increasing trends for most regions and seasons except winter, which could account for its leading role in corresponding seasons. R_n only showed significant trends in autumn and winter for most regions, which corresponded to its dominant position in these two seasons. Furthermore, the insignificant trends of u_2 in Region III for all seasons might also decipher its small contributions here. As shown in Figure 1, Region III is mainly a mountainous area with high elevation and the land use types are mainly forest and grassland. Meanwhile, Tao et al. [56] also found that the decreasing trend of u_2 of urban stations was significantly greater than that of rural stations in Anhui province, which could give a possible explanation for the insignificant upward trends of u_2 in Region III.

Although the effect of meteorological factors on ET_0 was well quantified in this study, some uncertainties still existed in this aspect. Firstly, the differential equation method was adopted in this study to determine the contribution of each meteorological factor to ET_0 trends. This method assumes that each major climate variable is independent and has been proven to be equivalent to the performance of the detrending method in a previous study [53]. However, each meteorological factor is not completely independent and may interact with one another, and the differential equation method adopts the averaged partial derivatives of each variable to attribute to the ET_0 changes, which may also introduce uncertainty in the ultimate results [67]. In addition, considering the complexity of the underlying surface, although the most complete observational data of national meteorological stations were employed in this study, the density of current meteorological stations was still sparse, which was not enough to fully reflect ET_0 changes and their causes at the spatial scale. Moreover, the changes in climate factors caused by human activities are likely to eventually lead to ET_0 changes. Therefore, human activities, especially land use and cover changes and urbanization, increase the errors and uncertainties of ET_0 calculation and attribution [31,68], which needs further research.

5. Conclusions

In this paper, we found that the ET_0 decreased significantly before 1990 (-3.89 mm·a^{-2}) and then increased slowly (0.62 mm·a^{-2}) throughout the Anhui province. Among the meteorological factors affecting ET_0 changes, T_a decreased significantly before 1990 and then increased significantly, with RH performing the opposite, while u_2 and R_n both declined significantly before 1990 and then slowed down. T_a, RH and R_n daily sensitivity coefficients to ET_0 increased first and then decreased, whereas u_2 showed a gradual change trend on the opposite. Generally, RH was the most sensitive factor except in summer, when R_n was the most sensitive factor. The four selected meteorological factors were reasonable and could explain well the contributions to ET_0 trends by employing the differential method. During 1961–1990, all meteorological factors provided negative contributions to ET_0 trends, which ultimately led to decreasing trends for almost all regions and periods. R_n was the leading factor annually, during the growing season and summer, while u_2 played a dominant role in other seasons. During 1991–2019, the leading factor of ET_0 trends changed to T_a annually, during the growing season, spring and summer, then to R_n in other seasons for most regions. T_a and RH exhibited positive contributions to ET_0 trends for most regions and periods, while u_2 and R_n showed negative contributions. Overall, the negative contributions from u_2 and R_n could not offset the positive contributions from T_a and RH, which, eventually, led to the slow upward ET_0 trends. Furthermore, the slightly increasing trends of u_2 and its extremely small contributions to the ET_0 trends in Region III deserve more attention. The outcomes obtained from this research should help in the understanding of the changing climate and provide a theoretical basis for the agricultural crop production and sustainable management of water resources in similar world regions.

Supplementary Materials: The following supporting information can be downloaded at: https://www.mdpi.com/article/10.3390/ijgi11050300/s1, Figure S1 Spatial distribution of dominant factors in Anhui province during 1961–1990, Figure S2 Spatial distribution of dominant factors in Anhui province during 1991–2019.

Author Contributions: Conceptualization, Meng Li, Ronghao Chu and Yuelin Jiang; Software, Xiuzhu Sha; Validation, Meng Li, Ronghao Chu and Yuelin Jiang; Formal Analysis, Meng Li and Ronghao Chu; Data Curation, Meng Li, Ronghao Chu and Xiuzhu Sha; Writing—Original Draft Preparation, Meng Li and Ronghao Chu; Supervision, Meng Li, Ronghao Chu and Yuelin Jiang; Funding Acquisition, Meng Li, Ronghao Chu and Yuelin Jiang; Writing—Review & Editing, Abu Reza Md. Towfiqul Islam, Yuelin Jiang and Shuanghe Shen. All authors have read and agreed to the published version of the manuscript.

Funding: This research was funded by the National Key Research and Development Program of China (2018YFD0300905), the Anhui Provincial Natural Science Foundation (1908085QD171; 2108085QD157), the National Natural Science Foundation of China (41905100), the Anhui Agricultural University Science Foundation for Young Scholars (2018zd07), the Anhui Agricultural University Introduction and Stabilization of Talent Fund (yj2018-57) and the Scientific Research Project of the Anhui Meteorological Bureau (KM202003).

Institutional Review Board Statement: Not applicable.

Informed Consent Statement: Not applicable.

Data Availability Statement: Not applicable.

Conflicts of Interest: The authors declare no conflict of interest.

References

1. Li, M.; Chu, R.; Shen, S.; Islam, A.R.M.T. Quantifying Climatic Impact on Reference Evapotranspiration Trends in the Huai River Basin of Eastern China. *Water* **2018**, *10*, 144. [CrossRef]
2. Chu, R.; Li, M.; Shen, S.; Islam, A.R.M.T.; Cao, W.; Tao, S.; Gao, P. Changes in Reference Evapotranspiration and Its Contributing Factors in Jiangsu, a Major Economic and Agricultural Province of Eastern China. *Water* **2017**, *9*, 486. [CrossRef]
3. Li, M.; Chu, R.; Shen, S.; Islam, A.R.M.T. Dynamic analysis of pan evaporation variations in the Huai River Basin, a climate transition zone in eastern China. *Sci. Total Environ.* **2018**, *625*, 496–509. [CrossRef] [PubMed]
4. Doorenbos, J.; Pruitt, W.O. Guidelines for Predicting Crop Water Requirements. In *FAO Irrigation and Drainage*; FAO: Rome, Italy, 1977.
5. Allen, R.G.; Pereira, L.S.; Raes, D.; Smith, M. Crop Evapotranspiration-Guidelines for Computing Crop Water Requirements. In *FAO Irrigation and Drainage Paper 56*; FAO: Rome, Italy, 1998.
6. Xiang, K.; Li, Y.; Horton, R.; Feng, H. Similarity and difference of potential evapotranspiration and reference crop evapotranspiration-a review. *Agric. Water Manag.* **2020**, *232*, 106043. [CrossRef]
7. Monteith, J.L. Evaporation and environment. *Symp. Soc. Exp. Biol.* **1965**, *19*, 205–234.
8. Allen, R.; Smith, M.; Pereira, L.; Perrier, A. An update for the calculation of reference evapotranspiration. *ICID Bull.* **1994**, *43*, 35–94.
9. Nijsse, F.; Cox, P.M.; Huntingford, C.; Williamson, M.S. Decadal global temperature variability increases strongly with climate sensitivity. *Nat. Clim. Chang.* **2019**, *9*, 598–601. [CrossRef]
10. Trenberth, K.E.; Dai, A.; van der Schrier, G.; Jones, P.D.; Barichivich, J.; Briffa, K.R.; Sheffield, J. Global warming and changes in drought. *Nat. Clim. Chang.* **2014**, *4*, 17–22. [CrossRef]
11. Islam, A.R.M.T.; Shen, S.; Yang, S.; Hu, Z.; Chu, R. Assessing recent impacts of climate change on design water requirement of Boro rice season in Bangladesh. *Theor. Appl. Climatol.* **2019**, *138*, 97–113. [CrossRef]
12. Nam, W.-H.; Hong, E.-M.; Choi, J.-Y. Has climate change already affected the spatial distribution and temporal trends of reference evapotranspiration in South Korea? *Agric. Water Manag.* **2015**, *150*, 129–138. [CrossRef]
13. Yassen, A.N.; Nam, W.-H.; Hong, E.-M. Impact of climate change on reference evapotranspiration in Egypt. *Catena* **2020**, *194*, 104711. [CrossRef]
14. Wang, Z.; Ye, A.; Wang, L.; Liu, K.; Cheng, L. Spatial and temporal characteristics of reference evapotranspiration and its climatic driving factors over China from 1979–2015. *Agric. Water Manag.* **2019**, *213*, 1096–1108. [CrossRef]
15. Pour, S.H.; Wahab, A.K.A.; Shahid, S.; Ismail, Z.B. Changes in reference evapotranspiration and its driving factors in peninsular Malaysia. *Atmos. Res.* **2020**, *246*, 105096. [CrossRef]
16. Maček, U.; Bezak, N.; Šraj, M. Reference evapotranspiration changes in Slovenia, Europe. *Agric. For. Meteorol.* **2018**, *260–261*, 183–192. [CrossRef]
17. Wang, Z.; Xie, P.; Lai, C.; Chen, X.; Wu, X.; Zeng, Z.; Li, J. Spatiotemporal variability of reference evapotranspiration and contributing climatic factors in China during 1961–2013. *J. Hydrol.* **2017**, *544*. [CrossRef]
18. Gao, Z.; He, J.; Dong, K.; Li, X. Trends in reference evapotranspiration and their causative factors in the West Liao River basin, China. *Agric. For. Meteorol.* **2017**, *232*, 106–117. [CrossRef]
19. Xu, C.Y.; Gong, L.; Jiang, T.; Chen, D.; Singh, V.P. Analysis of spatial distribution and temporal trend of reference evapotranspiration and pan evaporation in Changjiang (Yangtze River) catchment. *J. Hydrol.* **2006**, *327*, 81–93. [CrossRef]
20. Wang, W.; Shao, Q.; Peng, S.; Xing, W.; Yang, T.; Luo, Y.; Yong, B.; Xu, J. Reference evapotranspiration change and the causes across the Yellow River Basin during 1957–2008 and their spatial and seasonal differences. *Water Resour. Res.* **2012**, *48*, 1–27. [CrossRef]
21. Li, Z.; Li, Z.; Xu, Z.; Zhou, X. Temporal variations of reference evapotranspiration in Heihe River basin of China. *Hydrol. Res.* **2013**, *44*, 904–916. [CrossRef]
22. Huo, Z.; Dai, X.; Feng, S.; Kang, S.; Huang, G. Effect of climate change on reference evapotranspiration and aridity index in arid region of China. *J. Hydrol.* **2013**, *492*, 24–34. [CrossRef]
23. Nouri, M.; Homaee, M.; Bannayan, M. Quantitative trend, sensitivity and contribution analyses of reference evapotranspiration in some arid environments under climate change. *Water Resour. Manag.* **2017**, *31*, 2207–2224. [CrossRef]
24. Roderick, M.L.; Rotstayn, L.D.; Farquhar, G.D.; Hobbins, M.T. On the attribution of changing pan evaporation. *Geophys. Res. Lett.* **2007**, *34*, 251–270. [CrossRef]
25. Rotstayn, L.D.; Roderick, M.L.; Farquhar, G.D. A simple pan-evaporation model for analysis of climate simulations: Evaluation over Australia. *Geophys. Res. Lett.* **2006**, *33*, L17715. [CrossRef]
26. Shan, N.; Shi, Z.; Yang, X.; Gao, J.; Cai, D. Spatiotemporal trends of reference evapotranspiration and its driving factors in the Beijing-Tianjin Sand source control project region, China. *Agric. For. Meteorol.* **2015**, *200*, 322–333. [CrossRef]
27. Xu, L.; Shi, Z.; Wang, Y.; Zhang, S.; Chu, X.; Yu, P.; Xiong, W.; Zuo, H.; Wang, Y. Spatiotemporal variation and driving forces of reference evapotranspiration in Jing River Basin, northwest China. *Hydrol. Process.* **2015**, *29*, 4846–4862. [CrossRef]
28. Tang, B.; Tong, L.; Kang, S.; Zhang, L. Impacts of climate variability on reference evapotranspiration over 58 years in the Haihe river basin of north China. *Agric. Water Manag.* **2011**, *97*, 1506–1516. [CrossRef]

29. Li, C.; Wu, P.T.; Li, X.L.; Zhou, T.W.; Sun, S.K.; Wang, Y.B.; Luan, X.B.; Yu, X. Spatial and temporal evolution of climatic factors and its impacts on potential evapotranspiration in Loess Plateau of Northern Shaanxi, China. *Sci. Total Environ.* **2017**, *589*, 165–172. [CrossRef]
30. Wang, Q.; Wang, J.; Zhao, Y.; Li, H.; Zhai, J.; Yu, Z.; Zhang, S. Reference evapotranspiration trends from 1980 to 2012 and their attribution to meteorological drivers in the three-river source region, China. *Int. J. Climatol.* **2016**, *36*, 3759–3769. [CrossRef]
31. She, D.; Xia, J.; Zhang, Y. Changes in reference evapotranspiration and its driving factors in the middle reaches of Yellow River Basin, China. *Sci. Total Environ.* **2017**, *607–608*, 1151–1162. [CrossRef]
32. Vicente-Serrano, S.M.; Azorin-Molina, C.; Sanchez-Lorenzo, A.; Revuelto, J.; Moran-Tejeda, E.; Lopez-Moreno, J.I.; Espejo, F. Sensitivity of reference evapotranspiration to changes in meteorological parameters in Spain (1961–2011). *Water Resour. Res.* **2014**, *50*, 8458–8480. [CrossRef]
33. Dinpashoh, Y.; Jhajharia, D.; Fakheri-Fard, A.; Singh, V.P.; Kahya, E. Trends in reference crop evapotranspiration over Iran. *J. Hydrol.* **2011**, *399*, 422–433. [CrossRef]
34. Jerin, J.N.; Islam, H.M.T.; Islam, A.R.M.T.; Shahid, S.; Hu, Z.; Badhan, M.A.; Chu, R.; Elbeltagi, A. Spatiotemporal trends in reference evapotranspiration and its driving factors in Bangladesh. *Theor. Appl. Climatol.* **2021**, *144*, 793–808. [CrossRef]
35. Han, J.; Wang, J.; Zhao, Y.; Wang, Q.; Zhang, B.; Li, H.; Zhai, J. Spatio-temporal variation of potential evapotranspiration and climatic drivers in the Jing-Jin-Ji region, North China. *Agric. For. Meteorol.* **2018**, *256–257*, 75–83. [CrossRef]
36. Li, Z.; Chen, Y.; Shen, Y.; Liu, Y.; Zhang, S. Analysis of changing pan evaporation in the arid region of Northwest China. *Water Resour. Res.* **2013**, *49*, 2205–2212. [CrossRef]
37. Fan, Z.-X.; Thomas, A. Decadal changes of reference crop evapotranspiration attribution: Spatial and temporal variability over China 1960–2011. *J. Hydrol.* **2018**, *560*, 461–470. [CrossRef]
38. Zhang, L.; Traore, S.; Cui, Y.; Luo, Y.; Zhu, G.; Liu, B.; Fipps, G.; Karthikeyan, R.; Singh, V. Assessment of spatiotemporal variability of reference evapotranspiration and controlling climate factors over decades in China using geospatial techniques. *Agric. Water Manag.* **2019**, *213*, 499–511. [CrossRef]
39. Zhou, L.; Turvey, C.G. Climate change, adaptation and China's grain production. *China Econ. Rev.* **2014**, *28*, 72–89. [CrossRef]
40. Yang, H.; Hu, D.; Xu, H.; Zhong, X. Assessing the spatiotemporal variation of NPP and its response to driving factors in Anhui province, China. *Environ. Sci. Pollut. Res. Int.* **2020**, *27*, 14915–14932. [CrossRef]
41. Angstrom, A. Solar and terrestrial radiation. Report to the international commission for solar research on actinometric investigations of solar and atmospheric radiation. *Q. J. R. Meteorol. Soc.* **1924**, *50*, 121–126. [CrossRef]
42. Chen, R.; Kang, E.; Yang, J.; Lu, S.; Zhao, W. Validation of five global radiation models with measured daily data in China. *Energy Convers. Manag.* **2004**, *45*, 1759–1769. [CrossRef]
43. Hargreaves, G.H.; Samani, Z.A. Estimating potential evapotranspiration. *J. Irrig. Drain. Div.* **1982**, *108*, 225–230. [CrossRef]
44. Allen, R.G. Self-Calibrating Method for Estimating Solar Radiation from Air Temperature. *J. Hydrol.* **1997**, *2*, 56–67. [CrossRef]
45. Hargreaves, G.H.; Allen, R.G. History and evaluation of Hargreaves evapotranspiration equation. *J. Irrig. Drain. Eng.* **2003**, *129*, 53–63. [CrossRef]
46. McCuen, R.H. A sensitivity and error analysis of procedures used for estimating evaporation. *J. Am. Water Resour. Assoc.* **1974**, *10*, 486–497. [CrossRef]
47. Praveen, B.; Talukdar, S.; Shahfahad; Mahato, S.; Mondal, J.; Sharma, P.; Islam, A.R.M.T.; Rahman, A. Analyzing trend and forecasting of rainfall changes in India using non-parametrical and machine learning approaches. *Sci. Rep.* **2020**, *10*, 10342. [CrossRef] [PubMed]
48. Salam, R.; Islam, A.R.M.T.; Pham, Q.B.; Dehghani, M.; Al-Ansari, N.; Linh, N.T.T. The optimal alternative for quantifying reference evapotranspiration in climatic sub-regions of Bangladesh. *Sci. Rep.* **2020**, *10*, 20171. [CrossRef]
49. Islam, A.R.M.T.; Karim, M.R.; Mondol, M.A.H. Appraising trends and forecasting of hydroclimatic variables in the north and northeast regions of Bangladesh. *Theor. Appl. Climatol.* **2020**, *143*, 33–50. [CrossRef]
50. Theil, H. A Rank Invariant Method of Linear and Polynomial Regression Analysis. In *Advanced Studies in Theoretical and Applied Econometrics*; Nederlandse Akademie van Wetenschappen: Amsterdam, The Netherlands, 1950; Volume 23, pp. 345–381.
51. Sen, P.K. Estimates of the regression coefficient based on Kendall′s Tau. *J. Am. Stat. Assoc.* **1968**, *63*, 1379–1389. [CrossRef]
52. Ding, Y.; Ren, G.; Shi, G.; Gong, P.; Zheng, X.; Zhai, P.; Zhang, D.e.; Zhao, Z.; Wang, S.; Wang, H.; et al. National Assessment Report of Climate Change (I): Climate change in China and its future trend. *Adv. Clim. Chang. Res.* **2006**, *2*, 3–8.
53. Li, M.; Chu, R.; Islam, A.R.M.T.; Jiang, Y.; Shen, S. Attribution Analysis of Long-Term Trends of Aridity Index in the Huai River Basin, Eastern China. *Sustainability* **2020**, *12*, 1743. [CrossRef]
54. Matsoukas, C.; Benas, N.; Hatzianastassiou, N.; Pavlakis, K.G.; Kanakidou, M.; Vardavas, I. Potential evaporation trends over land between 1983–2008: Driven by radiative fluxes or vapour-pressure deficit? *Atmos. Chem. Phys.* **2011**, *11*, 7601–7616. [CrossRef]
55. Ren, G.; Guo, J.; Xu, M.; Chu, Z.; Zhang, L.; Zou, X.; Li, Q.; Liu, X. Climate changes of China′s mainland over the past half century. *J. Meteorol. Res.* **2005**, *63*, 942–956.
56. Tao, Y.; Huang, Y.; Yang, Y.; Wang, K.; Cheng, X.; Wang, M.; WU, R. Impact of urbanization on wind speed in Anhui province. *Clim. Chang. Res.* **2016**, *12*, 519–526.
57. Lin, C.; Yang, K.; Huang, J.; Tang, W.; Qin, J.; Niu, X.; Chen, Y.; Chen, D.; Lu, N.; Fu, R. Impacts of wind stilling on solar radiation variability in China. *Sci. Rep.* **2015**, *5*, 15135. [CrossRef]

58. Qian, Y.; Kaiser, D.P.; Leung, L.R.; Xu, M. More frequent cloud-free sky and less surface solar radiation in China from 1955 to 2000. *Geophys. Res. Lett.* **2006**, *33*, L01812. [CrossRef]
59. Ma, J.; Luo, Y.; Shen, Y.; Liang, H.; Li, S. Regional long-term trend of ground solar radiation in China over the past 50 years. *Sci. China Earth Sci.* **2012**, *42*, 1597–1608. [CrossRef]
60. Qi, Y.; Fang, S.; Zhou, W. Variation and spatial distribution of surface solar radiation in China over recent 50 years. *Acta Ecolog. Sin.* **2014**, *34*, 7444–7453.
61. Tao, S.; Qi, Y.; Shen, S.; Li, Y.; Zhou, Y. The spatial and temporal variation of solar radiation over China from 1981 to 2014. *J. Arid Land Res. Environ.* **2016**, *30*, 143–147.
62. Shan, N.; Shi, Z.; Yang, X.; Zhang, X.; Guo, H.; Zhang, B.; Zhang, Z. Trends in potential evapotranspiration from 1960 to 2013 for a desertification-prone region of China. *Int. J. Climatol.* **2016**, *36*, 3434–3445. [CrossRef]
63. Dong, Q.; Wang, W.; Shao, Q.; Xing, W.; Ding, Y.; Fu, J. The response of reference evapotranspiration to climate change in Xinjiang, China: Historical changes, driving forces, and future projections. *Int. J. Climatol.* **2020**, *40*, 235–254. [CrossRef]
64. Fan, J.; Wu, L.; Zhang, F.; Xiang, Y.; Zheng, J. Climate change effects on reference crop evapotranspiration across different climatic zones of China during 1956–2015. *J. Hydrol.* **2016**, *542*, 923–937. [CrossRef]
65. Wang, K.; Xu, Q.; Li, T. Does recent climate warming drive spatiotemporal shifts in functioning of high-elevation hydrological systems? *Sci. Total Environ.* **2020**, *719*, 137507. [CrossRef]
66. Yang, L.; Feng, Q.; Li, C.; Si, J.; Wen, X.; Yin, Z. Detecting climate variability impacts on reference and actual evapotranspiration in the Taohe River Basin, NW China. *Hydrol. Res.* **2016**, *48*, 596–612. [CrossRef]
67. Chu, R.; Li, M.; Islam, A.R.M.T.; Fei, D.; Shen, S. Attribution analysis of actual and potential evapotranspiration changes based on the complementary relationship theory in the Huai River basin of eastern China. *Int. J. Climatol.* **2019**, *39*, 4072–4090. [CrossRef]
68. Dong, Y.; Zhao, Y.; Zhai, J.; Zhao, J.; Han, J.; Wang, Q.; He, G.; Chang, H. Changes in reference evapotranspiration over the non-monsoon region of China during 1961–2017: Relationships with atmospheric circulation and attributions. *Int. J. Climatol.* **2021**, *41*, E734–E751. [CrossRef]